Colloidal Self-Assembly-Directed Laser-Induced Non-Close-Packed Crystalline Silicon Nanostructures

Kwan Wee Tan, Stacey A. Saba, Hitesh Arora,‡ Michael O. Thompson, and Ulrich Wiesner*

Department of Materials Science and Engineering, Cornell University, Ithaca, New York 14853, United States. ‡Present address: Intel Corporation, Chandler, Arizona 85226, United States.

ABSTRACT This report describes an ultrafast, large-area, and highly flexible method to construct complex two- and three-dimensional silicon nanostructures with deterministic non-close-packed symmetry. Pulsed excimer laser irradiation is used to induce a transient melt transformation of amorphous silicon filled in a colloidal self-assembly-directed inverse opal template, resulting in a nanostructured crystalline phase. The pattern transfer yields are high, and long-range order is maintained. This technique represents a potential route to obtain silicon nanostructures of various symmetries and associated unique properties for advanced applications such as energy storage and generation.

KEYWORDS: self-assembly · pulsed laser irradiation · colloidal crystals · silicon · crystalline · non-close-packed

Silicon-based nanomaterials have great potential for a wide variety of applications due to silicon's abundance and implicit compatibility with current semiconductor processing technologies. Structures based on silicon have been widely adapted as photonic crystals,[1−6] solar cells,[7−12] sensors,[13,14] and thermoelectric devices.[15−20] In particular, non-close-packed silicon nanostructures are highly desirable for their wide photonic band gap and may be beneficial for other surface-enhanced properties.[5,6,21−28]

Non-close-packed silicon nanostructures based on sacrificial inverse opal templates have been demonstrated, but only in the amorphous phase (a-Si).[5,6] While a myriad of methods to obtain crystalline silicon (c-Si) nanostructures exist, including, for example, slow heating of a-Si[2,3,10,29] and magnesium reduction of silica[4,30−32] (SiO_2) into c-Si at 600−675 °C, these thermal crystallization techniques in the solid phase require several hours at elevated temperatures in an inert environment. The stoichiometric yields of c-Si from magnesium reduction of SiO_2 are also relatively low (34.9 vol %).[30] An alternative approach is using pulsed lasers to induce an extremely short transient melt-crystallization conversion of a-Si precursors into c-Si, enabling thermal processing on many different substrates such as glass and polyimide.[33,34] Pulsed laser irradiation has been coupled to nanoimprinting,[35,36] nanosphere lithography,[37−39] and block copolymer-directed templating[40] to obtain Si nano-gratings, pillars, and porous thin films. To the best of our knowledge, however, it has not been applied to rapid transformations of colloidal crystal templates into non-close-packed c-Si structures.

In this work, we demonstrate a facile, rapid, and versatile method to fabricate non-close-packed c-Si colloidal nanostructures using a laser-induced transient melt process. We employed a hexagonally arranged close-packed (hcp) sacrificial colloidal crystal template to define and construct two-dimensional (2D) hexagonal-non-close-packed (hncp) c-Si arrays and 3D ordered macroporous hncp c-Si nanostructures. The crystallinity and non-close-packed symmetry of such highly ordered silicon 2D nanoarrays and 3D interconnecting pore network nanostructures are known to enhance electrical conductivity, photonic, and other surface properties significantly and could improve device performance, for example, in optoelectronics, photovoltaics, and thermoelectrics.[2,3,5,6,29]

RESULTS AND DISCUSSION

Scheme 1 illustrates the experimental processes. Polystyrene (PS) colloids (0.5 wt %) with diameters of either 530 or 350 nm were mixed with deionized water and hydrolyzed tetraethylorthosilicate (TEOS) solution.[32] A monolayer colloidal crystal of PS spheres surrounded by TEOS-derived SiO_2 was formed using the flow-controlled vertical deposition (FCVD) method.[41−43] The resulting latex beads were slowly calcined in air at 500 °C, leaving behind a highly ordered hcp SiO_2 inverse monolayer colloidal crystal. This inorganic template was subsequently filled with a ∼100 nm thick a-Si

* Address correspondence to ubw1@cornell.edu.

Received for review June 24, 2011 and accepted August 31, 2011.

Published online September 14, 2011
10.1021/nn2023446

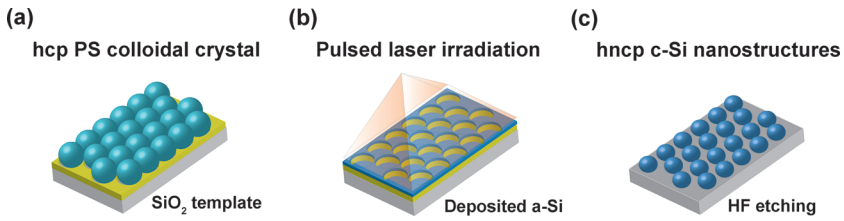

Scheme 1. Schematic illustration of hncp c-Si nanostructure generation. (a) The PS monolayer colloidal crystal surrounded by a SiO_2 matrix is grown using a one-step flow-controlled vertical deposition method on Si substrates. (b) PS beads are removed by slow calcination at 500 °C. a-Si is deposited as an overlayer on the hcp SiO_2 inverse colloidal crystal template and irradiated by a pulsed excimer laser. (c) The template is dissolved in HF, revealing the 2D hncp c-Si nanostructured arrays on the Si substrate

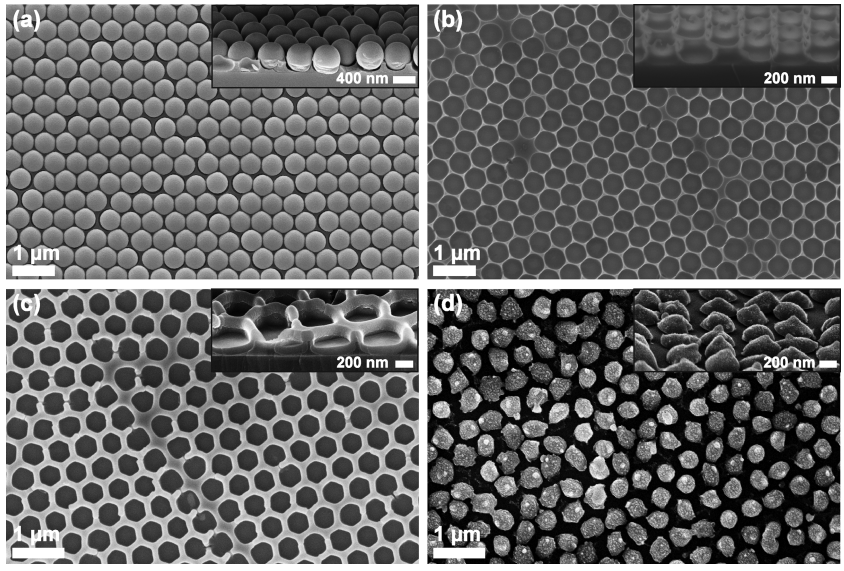

Figure 1. Plan view and cross-sectional (insets) SEM micrographs of the sputter-deposited and processed sample. (a) hcp PS monolayer colloidal crystal using 530 nm diameter beads surrounded by the SiO_2 matrix. (b) hcp SiO_2 inverse monolayer colloidal crystal template after calcination. (c) a-Si overlayer backfilled by top-down sputter deposition. (d) hncp c-Si nanostructures after HF etching.

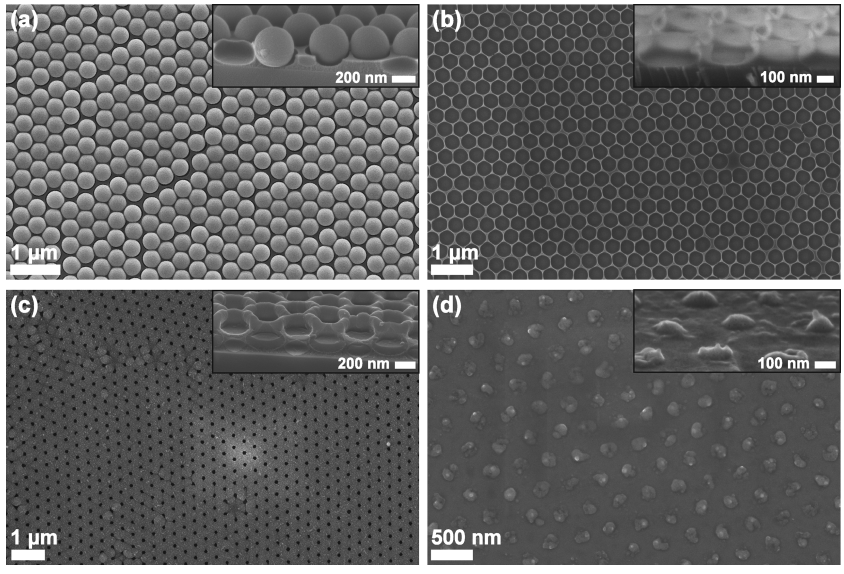

Figure 2. Plan view and cross-sectional (insets) SEM micrographs of samples formed and processed with PECVD a-Si deposition. (a) hcp PS monolayer colloidal crystal using 350 nm diameter beads surrounded by the SiO_2 matrix. (b) hcp SiO_2 inverse monolayer colloidal crystal after calcination. (c) a-Si overlayer deposited by PECVD. (d) hncp c-Si nanostructures after HF etching.

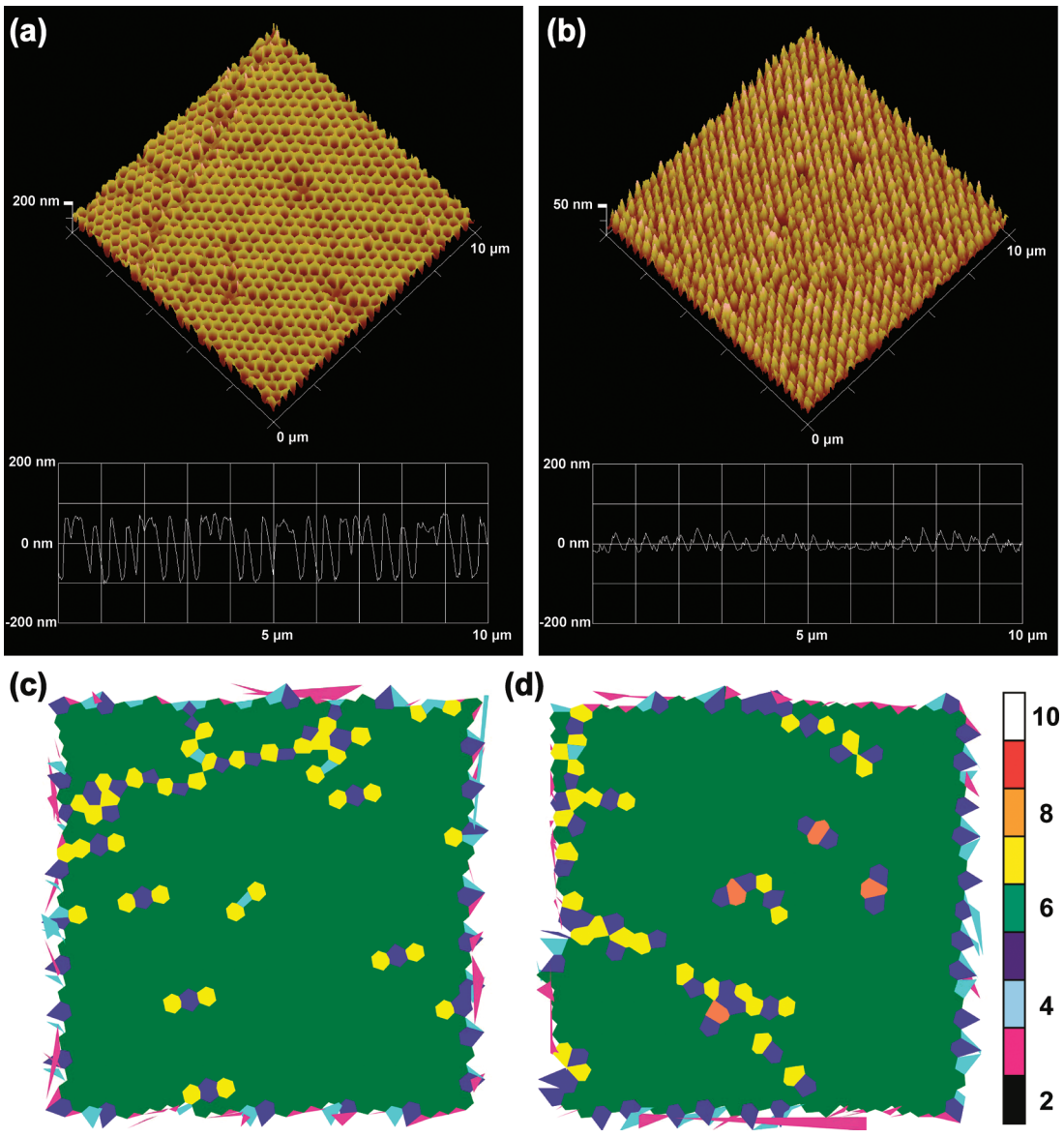

Figure 3. 3D AFM height profile images and corresponding Voronoi tessellation constructions of (a, c) the 350 nm hcp SiO_2 inverse monolayer colloidal crystal template and (b, d) the final hncp c-Si nanostructures of the PECVD sample. The vertical height axes range from (a) ±200 nm for the template and (b) ±50 nm for the c-Si nanostructures. The scan area for the AFM images and Voronoi analysis is 10 × 10 μm^2, and the color bar indicates the number of sides of the calculated polygon. The vast majority of the scan areas show 6-fold neighbors with only isolated defect regions.

overlayer by sputter deposition or plasma-enhanced chemical vapor deposition (PECVD) and irradiated with a 40 ns full-width-half-maximum pulsed XeCl excimer laser (308 nm wavelength) in air to induce the melt conversion of a-Si to the crystalline phase. The entire duration of laser-induced melt and solidification was approximately 20−100 ns. Finally, the SiO_2 template was removed in concentrated hydrofluoric (HF) acid solution, leaving the hncp Si nanostructured array seen in Scheme 1c.

Scanning electron microscopy (SEM) images in Figure 1 show the various stages of the process. A hcp SiO_2 inverse template (530 nm pore size, Figure 1b) obtained from PS monolayer colloidal crystal surrounded by a SiO_2 matrix (Figure 1a) was filled with ~100 nm of a-Si by top-down sputter deposition (Figure 1c). Melt of the a-Si overlayer was induced by a single 308 nm laser pulse at the single-crystal Si melt threshold of 600 mJ/cm^2 and rapidly solidified after 30 ns.[40] The SiO_2 template is transparent at this wavelength, and the laser irradiation energy is absorbed solely by Si. c-Si is formed when a-Si melts and solidifies as confirmed by characteristic time-resolved reflectance measurements (Figure S2 in the Supporting Information).[35,40,44,45] From Figure 1d the long-range hexagonal order of the resulting ncp c-Si nanostructured arrays was largely preserved after removing the template in an HF acid solution.

We postulate the c-Si nanostructure assumed the observed teardrop shape due to a combination of

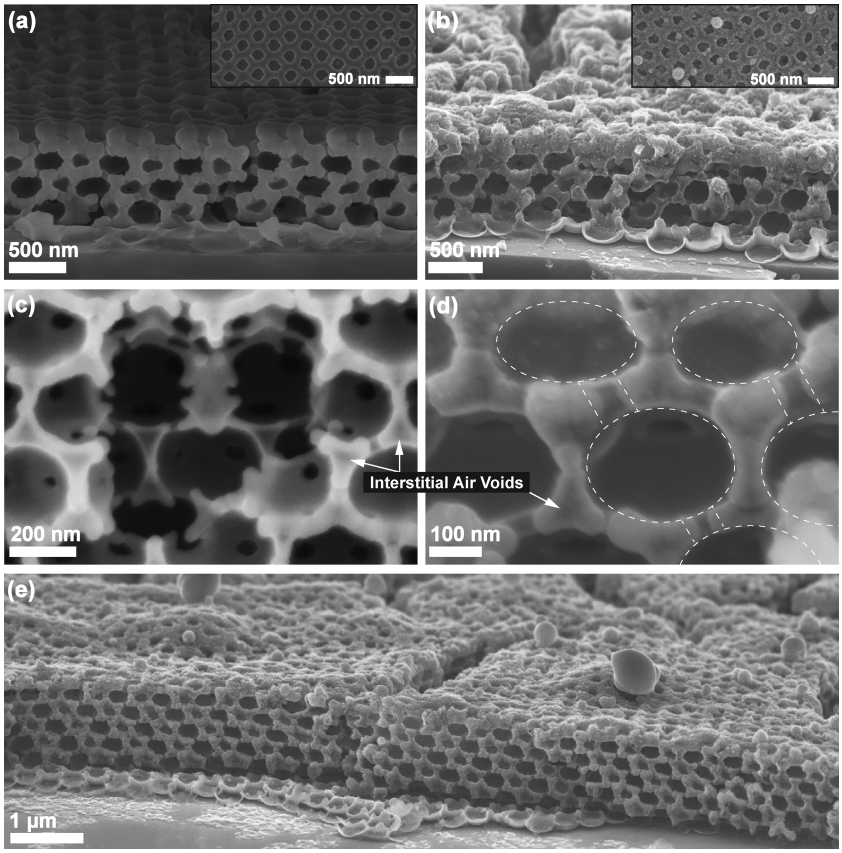

Figure 4. Cross-sectional and plan view (insets) SEM micrographs of (a) hncp SiO_2/a-Si core−shell composite inverse opal and (b) laser-induced hncp c-Si inverse opal nanostructures with four-monolayer periodicity after HF etching. Cross-sectional SEM images of (c) HF-etched a-Si inverse opal and (d) HF-etched laser-induced c-Si inverse opal nanostructures in high magnifications. The white-dotted region lines in part d highlight the quasi-cylindrical air channels connected to the quasi-spherical c-Si shells. (e) Cross-sectional SEM micrograph of laser-induced hncp c-Si inverse opal nanostructures with six-monolayer periodicity after HF etching.

template dewetting[46,47] and the rapid solidification process. Upon irradiation, a-Si in the SiO_2 pore melts and diffuses radially to the center driven by template dewetting. The molten Si would attempt to form a hemispherical shape to minimize the surface tension.[48] However, during this extremely short melt duration, the liquid Si (density of 2.53 g/cm^3) expands upon solidification (density of 2.30 g/cm^3) and perturbs the adjacent liquid Si, creating capillary waves.[34,49] These molten capillary waves are confined between coalescing solid grain boundaries from all directions and frozen into protruding ridge and hillock features with a teardrop shape as a result of heterogeneous nucleation and growth mechanism.[34,49] We also observe interconnected nanostructures (*e.g.*, see lower left corner in Figure 1d) that may be attributed to insufficient driving force and the ultrashort time scale for the liquid Si to dewet completely into the pores. From SEM data, the c-Si nanostructures are smaller than the pores, with an average width and height of around 410 and 300 nm, respectively, consistent with other experimental observations.[46]

SEM results from a smaller, 350 nm PS colloidal template (Figure 2a) are shown in Figure 2. A ∼100 nm thick a-Si film was deposited into the smaller SiO_2 inverse monolayer colloidal crystal template (Figure 2b) using PECVD. Figure 2c depicts hydrogenated a-Si deposited conformally within the pores and on the walls of the SiO_2 template. Due to the presence of hydrogen in PECVD a-Si films, microscopic blistering of the surface is observed for films irradiated at high fluences due to the explosive release of the trapped gas upon melting.[34,50,51] Alternatively, the hydrogenated a-Si films were irradiated with four sequential laser pulses at 500−700 mJ/cm^2, generating a more controlled and stepwise heating and release of hydrogen. The resulting hncp c-Si nanostructures imaged in Figures 2d with SEM and 3b with atomic force microscopy (AFM) exhibit an average width of around 170 nm and height of 60−70 nm.

Figure 3 shows the AFM height profile images and corresponding Voronoi tessellation constructions of both the hcp SiO_2 template and hncp c-Si nanostructured arrays resulting from the laser-induced melting and solidification process. An *n*-sided polygon represents a SiO_2 template pore or c-Si nanostructure at the center having an equivalent *n* number of nearest neighbors.[40,52,53] The majority green-colored hexagon

(6-fold) spatial areas in the Voronoi diagrams contain a total of 577 six-coordinated template pores (Figure 3c) and 571 six-coordinated c-Si nanostructures (Figure 3d) over a scan area of $10 \times 10\ \mu m^2$. Both the AFM results and Voronoi diagrams affirm quantitatively the hexagonal pattern transfer from the cp SiO_2 inverse colloidal template to the ncp c-Si nanostructures with almost 100% fidelity.

Beyond two dimensions, we applied the laser-induced transient melt process to obtain 3D ordered macroporous (3DOM) c-Si inverse opals with hncp symmetry based on micromolding in inverse silica opals (MISO).[5] We began with a multilayered SiO_2 inverse opal prepared by the FCVD method with 350 nm PS beads. Figure 4a shows the uniform deposition of hydrogenated a-Si by PECVD on the inner walls of the SiO_2 interconnected spherical cavities, yielding an hncp SiO_2/a-Si core−shell inverse colloidal crystal. The SiO_2/a-Si composite material was subsequently irradiated with a total of 43 sequential laser pulses at fluences from 5−550 mJ/cm^2. The low-energy fluences allowed for a slow and controlled release of hydrogen, while higher energies induced melt and converted the a-Si into c-Si, retaining the inverse opal morphology. The open structure and SiO_2 template walls reduced the melt threshold from 600 to 550 mJ/cm^2. Selective HF etching of the SiO_2 template results in an all c-Si single network of hncp inverse opal morphology seen with four- and six-monolayer periodicities in Figure 4b and e, respectively. Energy dispersive X-ray (EDX) analysis indicates that the resulting laser-induced c-Si 3DOM material consists almost entirely of silicon (<9% residual oxygen content, data not shown).

Figure 4c and d display high-magnification SEM micrographs of a-Si and c-Si inverse opals after HF etching, respectively. The darker contrast of the interstitial sites between three interconnecting quasi-spherical shells in both images suggests the placement of air voids that were formed after the removal of SiO_2 template and explicitly confirmed in the interior view of the a-Si inverse opal (Figure 4c). The white-dotted regions in Figure 4d highlight the quasi-cylindrical air channels connected to the quasi-spherical c-Si shells, a distinctive feature of hncp inverse opals.[5,6,25] From the SEM data, the quasi-spherical pore size in the laser-induced c-Si inverse opal material was reduced up to 40%, which can be attributed to the shrinkage of the SiO_2 template during calcination[23] and the thicker Si walls. This shrinkage is crucial to obtain the ncp symmetry. An interesting feature in the 3DOM nanostructures is the absence of dewetting of the molten Si from the SiO_2 pore walls. In contrast to the 2D nanoarrays, the absence of a clearly preferable single-crystal Si substrate could have resulted in the uniform a-Si melting within the porous structure.

For complete shape and structural control, we need to either fully dehydrogenate the PECVD a-Si film, deposit gas-free amorphous precursors, or irradiate *in situ* after deposition to reduce the total number of laser pulses and accumulated silicon melt duration. We postulate the best method is to achieve homogeneous nucleation and epitaxial growth of a single-crystal silicon nanostructure from the substrate.[40,54,55] In particular, we expect an interconnected and epitaxial ncp single-crystal 3D structure to facilitate optimal electrical charge transport properties and impart improved mechanical properties from the lack of grain boundaries. In analogy to results on block copolymer templates, this approach may be applied to form not only single-crystal homoepitaxial but also heteroepitaxial ncp nanostructured arrays on Si, enabling new functionalities and the engineering of novel device prototypes.[40]

CONCLUSION

In conclusion, we have performed the first experiments to demonstrate a highly rapid and versatile method using colloidal crystal templates coupled with pulsed excimer laser-induced melting to obtain ncp c-Si arrays of varying scales at ambient conditions. The resulting hncp c-Si nanostructured arrays maintain uniform separations and excellent long-range order as established by the hcp colloidal crystal template. Our results suggest a general strategy coupling soft-matter self-assembly with pulsed laser irradiation to direct and design intricate complex nanopatterned crystalline inorganic materials that could be used in advanced applications such as sensors, catalysis, and energy conversion.

METHODS

Colloidal Crystal Template Synthesis. PS colloids with diameters of 530 and 350 nm from Interfacial Dynamics and PolySciences, respectively, were used as received. Colloidal suspensions of 0.5 wt % were mixed in deionized water and hydrolyzed TEOS solution (TEOS/0.1 M HCl/EtOH, 1:1:1.5 by weight) as described elsewhere.[32] Si substrates used were cleaned with piranha solution (H_2SO_4/H_2O_2, 3:1 by volume) and rinsed profusely with deionized water before use. The PS colloidal crystal and surrounding SiO_2 matrix were grown on these substrates using the FCVD method.[41−43] The PS beads were removed by slow calcination at 500 °C for 2 h at a ramp rate of 2 °C/min in air. TEOS (98%, Sigma-Aldrich), HCl acid (37%, VWR), absolute EtOH (Pharmco), H_2SO_4 acid (97%, VWR), and H_2O_2 (30%, VWR) were used as received.

a-Si Deposition. a-Si was sputter-deposited into the 530 nm SiO_2 monolayer inverse opal template using a rf magnetron source with argon ions at a base pressure of 1.9×10^{-6} Torr and deposition rate of 9.8 nm/min for 10 min. a-Si was deposited into the 350 nm SiO_2 monolayer inverse opal template by PECVD at 400 °C for 2.2 min with a deposition rate of 46 nm/min. a-Si was deposited into the (350 nm) multilayered SiO_2

inverse opal template by PECVD at 400 °C for 3.3 min with a deposition rate of 46 nm/min.

Excimer Laser Irradiation. The laser irradiation setup is described elsewhere.[40] Briefly, a 40 ns full-width-half-maximum pulsed XeCl excimer laser (308 nm wavelength) was used to melt the a-Si in the SiO_2 template. Reflectance of the sample surface was monitored using a 650 nm diode laser. The laser-irradiated area on the sample was 3.2 × 3.2 mm. A single laser pulse of 600 mJ/cm^2 energy fluence was used to melt the 530 nm sputter-deposited a-Si monolayer sample. Four sequential laser pulses of 600, 700, 700, and 500 mJ/cm^2 energy fluences were used to melt the 350 nm PECVD a-Si monolayer sample. A total of 43 sequential laser pulses at fluences from 5 to 550 mJ/cm^2 were used to dehydrogenate and melt the 350 nm PECVD a-Si multilayered sample.

Template Removal. The sputter-deposited samples were treated in 20% HF acid solution, and PECVD samples were treated in 49% HF acid solution for 3−5 min to completely dissolve the SiO_2 templates.

Characterization. AFM images were obtained on a Veeco Nanoscope III in tapping mode with TappingMode Etched Si probes (325 kHz resonance frequency, 27 N/m force constant, 10 nm tip radius of curvature; all other values nominal) at ambient conditions. A LEO 1550 field emission SEM equipped with an in-lens detector and an EDX spectrometer (Quantax EDS, XFlash 3000 silicon drift detector, Bruker Nano GmbH) was used to image and identify the EDX signals of the samples. Voronoi tessellation diagrams were constructed using a self-written algorithm.[40,53]

Acknowledgment. The authors gratefully acknowledge a NSF creativity award (grant no. DMR-0605856) and support by the U.S. Department of Homeland Security under Cooperative Agreement Number 2009-ST-108-LR0004. K.W.T. gratefully acknowledges the Singapore Energy Innovation Programme Office for a National Research Foundation graduate fellowship. S. A.S. gratefully acknowledges Cornell University and the Semiconductor Research Corporation with support from Intel Foundation for an Engineering Learning Initiatives undergraduate research award. M.O.T. gratefully acknowledges financial support from Panasonic Corporation. The use of facilities of the Cornell Center for Materials Research, with funding from the Materials Research Science and Engineering Center program of NSF (under cooperative agreement no. DMR-0520404), and of the Cornell Nanoscale Science and Technology Facility supported by NSF (under grant no. ECS-0335765) is gratefully acknowledged. The authors also thank Prof. C. Liddell, J. Drewes, J. Drumheller, E. Riley, and H. Sai of Cornell University and Prof. Q. Yan of Tsinghua University for helpful discussions and kind experimental assistance.

Supporting Information Available: SEM micrographs of the laser-induced 3DOM hncp crystalline silicon nanostructures showing open quasi-spherical shells and time-resolved reflectance signal of sample. This information is available free of charge *via* the Internet at http://pubs.acs.org.

REFERENCES AND NOTES

1. Lin, S. Y.; Fleming, J. G.; Hetherington, D. L.; Smith, B. K.; Biswas, R.; Ho, K. M.; Sigalas, M. M.; Zubrzycki, W.; Kurtz, S. R.; Bur, J. A Three-Dimensional Photonic Crystal Operating at Infrared Wavelengths. *Nature* **1998**, *394*, 251–253.
2. Blanco, A.; Chomski, E.; Grabtchak, S.; Ibisate, M.; John, S.; Leonard, S. W.; Lopez, C.; Meseguer, F.; Miguez, H.; Mondia, J. P.; *et al.* Large-Scale Synthesis of a Silicon Photonic Crystal with a Complete Three-Dimensional Bandgap near 1.5 Micrometres. *Nature* **2000**, *405*, 437–440.
3. Vlasov, Y. A.; Bo, X.-Z.; Sturm, J. C.; Norris, D. J. On-Chip Natural Assembly of Silicon Photonic Bandgap Crystals. *Nature* **2001**, *414*, 289–293.
4. Ibisate, M.; Golmayo, D.; López, C. Silicon Direct Opals. *Adv. Mater.* **2009**, *21*, 2899–2902.
5. Míguez, H.; Tétreault, N.; Yang, S. M.; Kitaev, V.; Ozin, G. A. A New Synthetic Approach to Silicon Colloidal Photonic Crystals with a Novel Topology and an Omni-Directional Photonic Bandgap: Micromolding in Inverse Silica Opal (MISO). *Adv. Mater.* **2003**, *15*, 597–600.
6. Blanco, A.; López, C. Silicon Onion-Layer Nanostructures Arranged in Three Dimensions. *Adv. Mater.* **2006**, *18*, 1593–1597.
7. Tian, B.; Zheng, X.; Kempa, T. J.; Fang, Y.; Yu, N.; Yu, G.; Huang, J.; Lieber, C. M. Coaxial Silicon Nanowires as Solar Cells and Nanoelectronic Power Sources. *Nature* **2007**, *449*, 885–889.
8. Garnett, E. C.; Yang, P. Silicon Nanowire Radial p−n Junction Solar Cells. *J. Am. Chem. Soc.* **2008**, *130*, 9224–9225.
9. Kelzenberg, M. D.; Boettcher, S. W.; Petykiewicz, J. A.; Turner-Evans, D. B.; Putnam, M. C.; Warren, E. L.; Spurgeon, J. M.; Briggs, R. M.; Lewis, N. S.; Atwater, H. A. Enhanced Absorption and Carrier Collection in Si Wire Arrays for Photovoltaic Applications. *Nat. Mater.* **2010**, *9*, 239–244.
10. Suezaki, T.; Chen, J. I. L.; Hatayama, T.; Fuyuki, T.; Ozin, G. A. Electrical Properties of p-Type and n-Type Doped Inverse Silicon Opals - Towards Optically Amplified Silicon Solar Cells. *Appl. Phys. Lett.* **2010**, *96*, 242102.
11. Taira, K.; Nakata, J. Silicon Cells: Catching Rays. *Nat. Photon.* **2010**, *4*, 602–603.
12. Xu, S.; Huang, S. Y.; Levchenko, I.; Zhou, H. P.; Wei, D. Y.; Xiao, S. Q.; Xu, L. X.; Yan, W. S.; Ostrikov, K. Highly Efficient Silicon Nanoarray Solar Cells by a Single-Step Plasma-Based Process. *Adv. Energy Mater.* **2011**, *1*, 373–376.
13. Lin, V. S.-Y.; Motesharei, K.; Dancil, K.-P. S.; Sailor, M. J.; Ghadiri, M. R. A Porous Silicon-Based Optical Interferometric Biosensor. *Science* **1997**, *278*, 840–843.
14. Cui, Y.; Wei, Q.; Park, H.; Lieber, C. M. Nanowire Nanosensors for Highly Sensitive and Selective Detection of Biological and Chemical Species. *Science* **2001**, *293*, 1289–1292.
15. Li, D.; Wu, Y.; Kim, P.; Shi, L.; Yang, P.; Majumdar, A. Thermal Conductivity of Individual Silicon Nanowires. *Appl. Phys. Lett.* **2003**, *83*, 2934.
16. Boukai, A. I.; Bunimovich, Y.; Tahir-Kheli, J.; Yu, J.-K.; Goddard, W. A., III; Heath, J. R. Silicon Nanowires as Efficient Thermoelectric Materials. *Nature* **2008**, *451*, 168–171.
17. Hochbaum, A. I.; Chen, R.; Delgado, R. D.; Liang, W.; Garnett, E. C.; Najarian, M.; Majumdar, A.; Yang, P. Enhanced Thermoelectric Performance of Rough Silicon Nanowires. *Nature* **2008**, *451*, 163–167.
18. Lee, J.-H.; Galli, G. A.; Grossman, J. C. Nanoporous Si as an Efficient Thermoelectric Material. *Nano Lett.* **2008**, *8*, 3750–3754.
19. Yu, J.-K.; Mitrovic, S.; Tham, D.; Varghese, J.; Heath, J. R. Reduction of Thermal Conductivity in Phononic Nanomesh Structures. *Nat. Nanotechnol.* **2010**, *5*, 718–721.
20. Tang, J.; Wang, H.-T.; Lee, D. H.; Fardy, M.; Huo, Z.; Russell, T. P.; Yang, P. Holey Silicon as an Efficient Thermoelectric Material. *Nano Lett.* **2010**, *10*, 4279–4283.
21. Li, Y.; Cai, W.; Duan, G. Ordered Micro/Nanostructured Arrays Based on the Monolayer Colloidal Crystals. *Chem. Mater.* **2008**, *20*, 615–624.
22. Zhang, J.; Li, Y.; Zhang, X.; Yang, B. Colloidal Self-Assembly Meets Nanofabrication: From Two-Dimensional Colloidal Crystals to Nanostructure Arrays. *Adv. Mater.* **2010**, *22*, 4249–4269.
23. Stein, A.; Li, F.; Denny, N. R. Morphological Control in Colloidal Crystal Templating of Inverse Opals, Hierarchical Structures, and Shaped Particles. *Chem. Mater.* **2008**, *20*, 649–666.
24. Fenollosa, R.; Meseguer, F. Non-Close-Packed Artificial Opals. *Adv. Mater.* **2003**, *15*, 1282–1285.
25. King, J. S.; Gaillot, D. P.; Graugnard, E.; Summers, C. J. Conformally Back-Filled, Non-Close-Packed Inverse-Opal Photonic Crystals. *Adv. Mater.* **2006**, *18*, 1063–1067.
26. Li, Y.; Sasaki, T.; Shimizu, Y.; Koshizaki, N. A Hierarchically Ordered TiO_2 Hemispherical Particle Array with Hexagonal-Non-Close-Packed Tops: Synthesis and Stable Superhydrophilicity without UV Irradiation. *Small* **2008**, *4*, 2286–2291.

27. Gao, S.; Koshizaki, N.; Li, Y.; Li, L. Unique Hexagonal Non-Close-Packed Arrays of Alumina Obtained by Plasma Etching/Deposition with Catalytic Performance. *J. Mater. Chem.* **2011**, *21*, 2087.
28. Isa, L.; Kumar, K.; Müller, M.; Grolig, J.; Textor, M.; Reimhult, E. Particle Lithography from Colloidal Self-Assembly at Liquid−Liquid Interfaces. *ACS Nano* **2010**, *4*, 5665–5670.
29. Suezaki, T.; O'Brien, P. G.; Chen, J. I. L.; Loso, E.; Kherani, N. P.; Ozin, G. A. Tailoring the Electrical Properties of Inverse Silicon Opals - A Step Towards Optically Amplified Silicon Solar Cells. *Adv. Mater.* **2009**, *21*, 559–563.
30. Bao, Z.; Weatherspoon, M. R.; Shian, S.; Cai, Y.; Graham, P. D.; Allan, S. M.; Ahmad, G.; Dickerson, M. B.; Church, B. C.; Kang, Z.; *et al*. Chemical Reduction of Three-Dimensional Silica Micro-Assemblies into Microporous Silicon Replicas. *Nature* **2007**, *446*, 172–175.
31. Richman, E. K.; Kang, C. B.; Brezesinski, T.; Tolbert, S. H. Ordered Mesoporous Silicon through Magnesium Reduction of Polymer Templated Silica Thin Films. *Nano Lett.* **2008**, *8*, 3075–3079.
32. Hatton, B.; Mishchenko, L.; Davis, S.; Sandhage, K. H.; Aizenberg, J. Assembly of Large-Area, Highly Ordered, Crack-Free Inverse Opal Films. *Proc. Natl. Acad. Sci. U. S. A.* **2010**, *107*, 10354–10359.
33. Poate, J. M.; Mayer, J. W. *Laser Annealing of Semiconductors*; Academic Press: New York, 1982.
34. Street, R. *Technology and Applications of Amorphous Silicon*; Springer: New York, 2000.
35. Chou, S. Y.; Keimel, C.; Gu, J. Ultrafast and Direct Imprint of Nanostructures in Silicon. *Nature* **2002**, *417*, 835–837.
36. Mendu, K. K.; Shi, J.; Lu, Y. F.; Li, L. P.; Batta, N.; Doerr, D. W.; Alexander, D. R. Fabrication of Multi-Layered Inverse Opals Using Laser-Assisted Imprinting. *Nanotechnology* **2005**, *16*, 1965–1968.
37. Lu, Y.; Chen, S. C. Nanopatterning of a Silicon Surface by Near-Field Enhanced Laser Irradiation. *Nanotechnology* **2003**, *14*, 505–508.
38. Brodoceanu, D.; Landström, L.; Bäuerle, D. Laser-Induced Nanopatterning of Silicon with Colloidal Monolayers. *Appl. Phys. A: Mater. Sci. Process.* **2006**, *86*, 313–314.
39. Li, L.; Guo, W.; Wang, Z. B.; Liu, Z.; Whitehead, D.; Luk'yanchuk, B. Large-Area Laser Nano-Texturing with User-Defined Patterns. *J. Micromech. Microeng.* **2009**, *19*, 054002.
40. Arora, H.; Du, P.; Tan, K. W.; Hyun, J. K.; Grazul, J.; Xin, H. L.; Muller, D. A.; Thompson, M. O.; Wiesner, U. Block Copolymer Self-Assembly−Directed Single-Crystal Homo- and Heteroepitaxial Nanostructures. *Science* **2010**, *330*, 214–219.
41. Zhou, Z.; Zhao, X. S. Opal and Inverse Opal Fabricated with a Flow-Controlled Vertical Deposition Method. *Langmuir* **2005**, *21*, 4717–4723.
42. Tan, K. W.; Li, G.; Koh, Y. K.; Yan, Q.; Wong, C. C. Layer-by-Layer Growth of Attractive Binary Colloidal Particles. *Langmuir* **2008**, *24*, 9273–9278.
43. Tan, K. W.; Koh, Y. K.; Chiang, Y.-M.; Wong, C. C. Particulate Mobility in Vertical Deposition of Attractive Monolayer Colloidal Crystals. *Langmuir* **2010**, *26*, 7093–7100.
44. Auston, D. H.; Surko, C. M.; Venkatesan, T. N. C.; Slusher, R. E.; Golovchenko, J. A. Time-Resolved Reflectivity of Ion-Implanted Silicon During Laser Annealing. *Appl. Phys. Lett.* **1978**, *33*, 437.
45. Thompson, M. O.; Galvin, G. J.; Mayer, J. W.; Peercy, P. S.; Poate, J. M.; Jacobson, D. C.; Cullis, A. G.; Chew, N. G. Melting Temperature and Explosive Crystallization of Amorphous Silicon During Pulsed Laser Irradiation. *Phys. Rev. Lett.* **1984**, *52*, 2360.
46. Giermann, A. L.; Thompson, C. V. Solid-State Dewetting for Ordered Arrays of Crystallographically Oriented Metal Particles. *Appl. Phys. Lett.* **2005**, *86*, 121903.
47. Oh, Y.-J.; Ross, C. A.; Jung, Y. S.; Wang, Y.; Thompson, C. V. Cobalt Nanoparticle Arrays Made by Templated Solid-State Dewetting. *Small* **2009**, *5*, 860–865.
48. Li, J. G.; Hausner, H. Wetting and Adhesion in Liquid Silicon/Ceramic Systems. *Mater. Lett.* **1992**, *14*, 329–332.
49. Fork, D. K.; Anderson, G. B.; Boyce, J. B.; Johnson, R. I.; Mei, P. Capillary Waves in Pulsed Excimer Laser Crystallized Amorphous Silicon. *Appl. Phys. Lett.* **1996**, *68*, 2138.
50. Mei, P.; Boyce, J. B.; Hack, M.; Lujan, R. A.; Johnson, R. I.; Anderson, G. B.; Fork, D. K.; Ready, S. E. Laser Dehydrogenation/Crystallization of Plasma-Enhanced Chemical Vapor Deposited Amorphous Silicon for Hybrid Thin Film Transistors. *Appl. Phys. Lett.* **1994**, *64*, 1132.
51. McCulloch, D. J.; Brotherton, S. D. Surface Roughness Effects in Laser Crystallized Polycrystalline Silicon. *Appl. Phys. Lett.* **1995**, *66*, 2060.
52. Riley, E. K.; Liddell, C. M. Confinement-Controlled Self Assembly of Colloids with Simultaneous Isotropic and Anisotropic Cross-Section. *Langmuir* **2010**, *26*, 11648–11656.
53. Voronoi and Nearest Neighbor Pattern Analysis Algorithms. http://people.ccmr.cornell.edu/~uli/pages/idl.htm (accessed Mar 11, 2011).
54. Hu, S.; Leu, P. W.; Marshall, A. F.; McIntyre, P. C. Single-Crystal Germanium Layers Grown on Silicon by Nanowire Seeding. *Nat. Nanotechnol.* **2009**, *4*, 649–653.
55. Nelson, E. C.; Dias, N. L.; Bassett, K. P.; Dunham, S. N.; Verma, V.; Miyake, M.; Wiltzius, P.; Rogers, J. A.; Coleman, J. J.; Li, X.; *et al*. Epitaxial Growth of Three-Dimensionally Architectured Optoelectronic Devices. *Nat. Mater.* **2011** [Advance Online Publication]. DOI: 10.1038/nmat3071. Published online: July 24, 2011.